Structure, Vol. 12, 1947–1954, November, 2004, ©2004 Elsevier Ltd. All rights reserved. DOI 10.1016/j.str.2004.09.008

An Alternate Conformation and a Third Metal in PstP/Ppp, the *M. tuberculosis* PP2C-Family Ser/Thr Protein Phosphatase

Kristi E. Pullen, Ho-Leung Ng, Pei-Yi Sung, Matthew C. Good,[1] Stephen M. Smith,[2] and Tom Alber*
Department of Molecular and Cell Biology
339 Hildebrand Hall #3206
University of California, Berkeley
Berkeley, California 94720

Summary

Serine/threonine protein phosphatases are central mediators of phosphorylation-dependent signals in eukaryotes and a variety of pathogenic bacteria. Here, we report the crystal structure of the intracellular catalytic domain of *Mycobacterium tuberculosis* PstPpp, a membrane-anchored phosphatase in the PP2C family. Despite sharing the fold and two-metal center of human PP2Cα, the PstPpp catalytic domain binds a third Mn^{2+} in a site created by a large shift in a previously unrecognized flap subdomain adjacent to the active site. Mutations in this site selectively increased the Michaelis constant for Mn^{2+} in the reaction of a noncognate, small-molecule substrate, p-nitrophenyl phosphate. The PstP/Ppp structure reveals core functional motifs that advance the framework for understanding the mechanisms of substrate recognition, catalysis, and regulation of PP2C phosphatases.

Introduction

Reversible protein phosphorylation provides a ubiquitous signaling mechanism that alters cellular metabolism in response to changing conditions. In eukaryotes, Ser, Thr, or Tyr residues in approximately one-third of proteins are the targets of phosphorylation. The actions of protein kinases are reversed by protein phosphatases, and precise regulation and targeting of protein kinases and phosphatases are essential to achieve metabolic control. The human genome encodes over 130 putative protein phosphatases, including about 100 in protein tyr phosphatase and dual-specificity classes and about 30 Ser/Thr phosphatases (Bhaduri and Sowdhamini, 2003; Wang et al., 2003). The Ser/Thr phosphatases are greatly expanded in plants, including *A. thaliana*, which contains only one predicted protein tyr phosphatase, 18 candidate dual-specificity phosphatases, and 92 predicted Ser/Thr phosphatases (Kerk et al., 2002). Based on sequence motifs, Ser/Thr phosphatases are divided into the PPP and PPM families, with the PP1, PP2A, and PP2B phosphatases included in the PPP family (Barford et al., 1998). The prototypical member of the PPM family is PP2C, which differs from the PPP enzymes in its dependence on the divalent cations Mg^{2+} or Mn^{2+} as well as its resistance to classical PPP inhibitors such as okadaic acid. PP2C phosphatases negatively regulate a variety of signaling pathways, including the stress response, the *Wnt* pathway, and the cystic fibrosis conductance regulator (summarized in Jackson et al., 2003). PP2C enzymes also antagonize the signals of members of the large family (>600 in *A. thaliana*) of receptor-like kinases in plants (McCarty and Chory, 2000).

The mechanism of action of PP2C phosphatases is understood in terms of a single crystal structure, that of human PP2Cα in complex with the product, phosphate (Das et al., 1996). The PP2C fold comprises a central β sandwich surrounded by α helices. Four conserved Asp residues, a Glu, and a backbone carbonyl of Gly form a binding site for two adjacent Mn^{2+} ions and six water molecules. The octahedrally coordinated Mn^{2+} ions share an equatorial hydroxide ion or water molecule, which functions as the nucleophile that attacks the substrate phosphoryl group in a concerted hydrolytic reaction (Das et al., 1996; Jackson and Denu, 2001; Fjeld and Denu, 1999). A conserved Arg residue is positioned to form hydrogen bonds with the product phosphate. A large, irregular flap joining two β strands forms one side of a cleft containing the two-metal center.

To test the generality of this framework, we determined the crystal structure of PstP/Ppp, the single, broad-specificity PP2C-family Ser/Thr phosphatase domain encoded in the genome of *Mycobacterium tuberculosis* (*Mtb*, Cole et al., 2000). PstP (Boitel et al., 2003) is also known as Rv0018c (Cole et al., 2000), Ppp (Cole et al., 2000), and Mstp (Chopra et al, 2003). We adopted the name PstP because the name Ppp incorrectly links this PPM protein to the PPP protein phosphatase family.

Mtb is the causative agent of tuberculosis, the leading infectious disease worldwide, causing over two million deaths annually (Russell, 2001). PstP dephosphorylates the targets of the 11 predicted Ser/Thr protein kinases (STPKs) in *Mtb* (Boitel et al., 2003, Chopra et al., 2003), which mediate as yet undefined, essential, developmental and metabolic signals in response to unknown environmental cues (Av-Gay and Everett, 2000). The PknG STPK was recently reported to be secreted into host macrophages and to promote virulence by inhibiting fusion of lysosomes with phagosomes harboring the bacteria (Walburger et al., 2004). The *Mtb* STPKs and PstP are representative of a widespread class of eukaryotic-like STPK systems discovered in recent years in a growing number of bacterial species, including dozens of human pathogens (Kennelly, 2002). The shared features in the structures of PstP and PP2Cα define the core elements of the PPM family. In contrast to the human enzyme, however, PstP binds a third Mn^{2+} in the active site, and a flap subdomain is globally repositioned to contact this third Mn^{2+}. We propose that this Mn^{2+} ion may define the metal dependence of activity or help mediate recognition of protein substrates.

*Correspondence: tom@ucxray.berkeley.edu
[1]Present address: Department of Biochemistry and Biophysics, University of California, San Francisco, California 94143.
[2]Present address: Department of Chemistry, Northwestern University, Evanston, Illinois 60208.

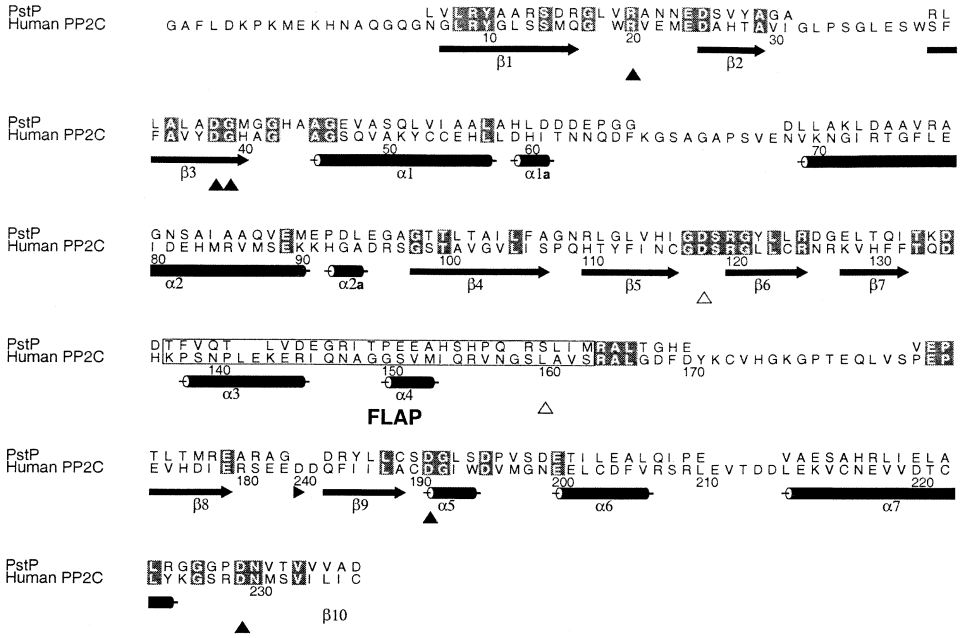

Figure 1. Structure-Based Sequence Alignment of *Mtb* PstP and Human PP2Cα Catalytic Domains

PstP β strands (arrows) and α helices (cylinders) are indicated below the sequences. Numbering corresponds to PstP. Residues that form the conserved two-metal center (black triangles) and the PstP Mn3 site (open triangles) are indicated. The flap sequences are boxed. Identical residues are highlighted in gray. No significant homologies were detected by BLAST beyond PstP residue 235.

Results and Discussion

PstP Fold

Mtb PstP contains a predicted intracellular phosphatase domain (Kelley et al., 2000) (Figure 1) joined by a segment with low sequence complexity to a single presumptive transmembrane helix and a 191 residue extracellular domain. The structure of the 237 residue phosphatase domain, defined by homology to bacterial PP2C family members, was determined using multiwavelength anomalous diffraction at 1.95 Å resolution (Table 1; Figure 2). The similarity of the two independent monomers in the asymmetric unit (backbone root-mean-square deviation [rmsd] of 0.52 Å) indicated that a representative conformation was observed. The PstP crystals hydrolyzed the small-molecule substrate, *p*-nitrophenyl phosphate (pNPP), in mother liquor at pH 7.5 (data not shown). This activity suggested that the structure represents an active con-

Table 1. Data Collection, Phasing, and Refinement Statistics for the PstP Phosphatase Domain

Data Collection and Phasing				
Crystal symmetry and unit cell	$P2_1$, a = 67.64 Å	b = 58.76 Å	c = 73.82 Å	β = 102.15°
Wavelength (Å)	1.12714	0.97960	0.95373	1.8926 (Mn f″)
Resolution (Å)	72.6–1.95	72.6–1.95	72.6–1.95	72.6–2.270
Completeness %[a]	98.0 (87.4)	99.4 (98.8)	96.4 (72.4)	97.8 (95.7)
Multiplicity	3.5 (2.2)	2.0 (2.0)	3.5 (2.2)	9.1 (8.8)
R_{merge} (%)[b]	6.0 (41.5)	6.8 (34.9)	9.7 (44.6)	10.9 (66.0)
$\langle I/\sigma I \rangle$[†]	26.1 (1.90)	12.8 (2.31)	13.5 (1.75)	12.1 (5.1)
Mean figure of merit[c]	0.39; 0.58 after solvent flattening			
Refinement				
Resolution (Å)	72.6–1.95			
Reflections	38,658			
R_{cryst}/R_{free} (%)[d]	0.200/0.230			
Rms Δ bonds, Δ angles[e]	0.008 Å, 1.092°			
Average B factor (Å^2)	29.5			
Main chain dihedral angles	most favored, 95.3%; allowed, 4.7%			

[a] Parentheses denote values for the highest resolution shell.

[b] $R_{merge} = \Sigma|I - \langle I \rangle|/\Sigma I$; *I*, intensity.

[c] Mean figure of merit $= \langle|\Sigma_\alpha P(\alpha) e_{i\alpha}/\Sigma_\alpha P(\alpha)|\rangle$; α, phase; P(α), phase probability distribution.

[d] $R_{cryst} = \Sigma|F_o - F_{calc}|/\Sigma F_o$; F_o, observed structure-factor amplitude; F_{calc}, calculated structure-factor amplitude.

[e] Root-mean-square deviations from ideal values.

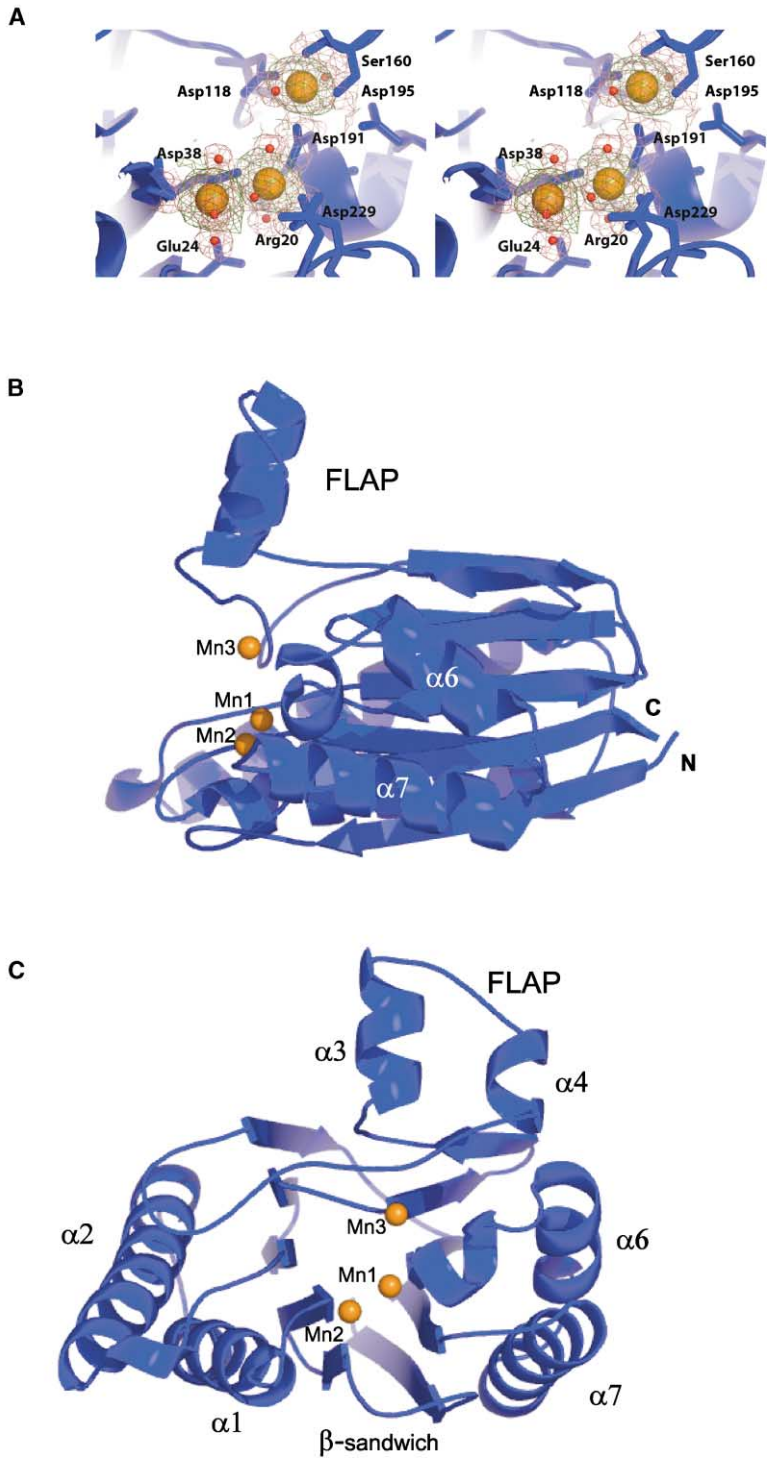

Figure 2. *Mtb* PstP Catalytic Domain Forms a β Sandwich that Binds Three Mn^{2+} Ions

(A) Stereo view of the active site superimposed on the MAD-phased, 1.95 Å resolution electron density map contoured at 1σ (teal) around the metal ions (orange) and bound water molecules (red). Also shown is the anomalous difference electron density map (2.27 Å resolution, 3σ, magenta) calculated with data collected at the Mn absorbtion peak. The difference electron density features identify the metal ions as Mn^{2+}.

(B) Ribbon diagram of the PstP phosphatase domain showing the β sandwich motif. The active site metals (orange) are located at the end (left) of the two, five-stranded, antiparallel β sheets. The N terminus is adjacent to the C terminus on the other side (right) of the β sandwich. In this view, the flap extends above the β sandwich and contacts Mn3.

(C) View into the active site of the PstP phosphatase domain (perpendicular to Figure 3B) shows the alternating helix-sheet-sheet-helix layers of the β sandwich. The N and C termini occur at the back of the figure. The three Mn^{2+} ions (orange) are bound in the active site. Ser160 (not shown, see Figure 3C) in the PstP flap (top) provides two direct ligands to Mn3.

formation or that any motions associated with catalysis are tolerated in the crystal lattice.

Because the PstP and human PP2Cα phosphatase domains share only 17% sequence identity (Figure 1), comparison of these three-dimensional structures brings into sharp focus the essential elements of this protein family. The core secondary structural elements and their topology are conserved in the *Mtb* and human PP2C catalytic domains. The common elements include a central β sandwich comprised of two five-stranded, antiparallel β sheets, each flanked by a pair of antiparallel helices (Figure 2).

Despite this overall structural similarity, several large differences are apparent (Figure 3). Globally, PstP is missing the first β strand and the entire C-terminal, helical domain of the human phosphatase (Das et al., 1996).

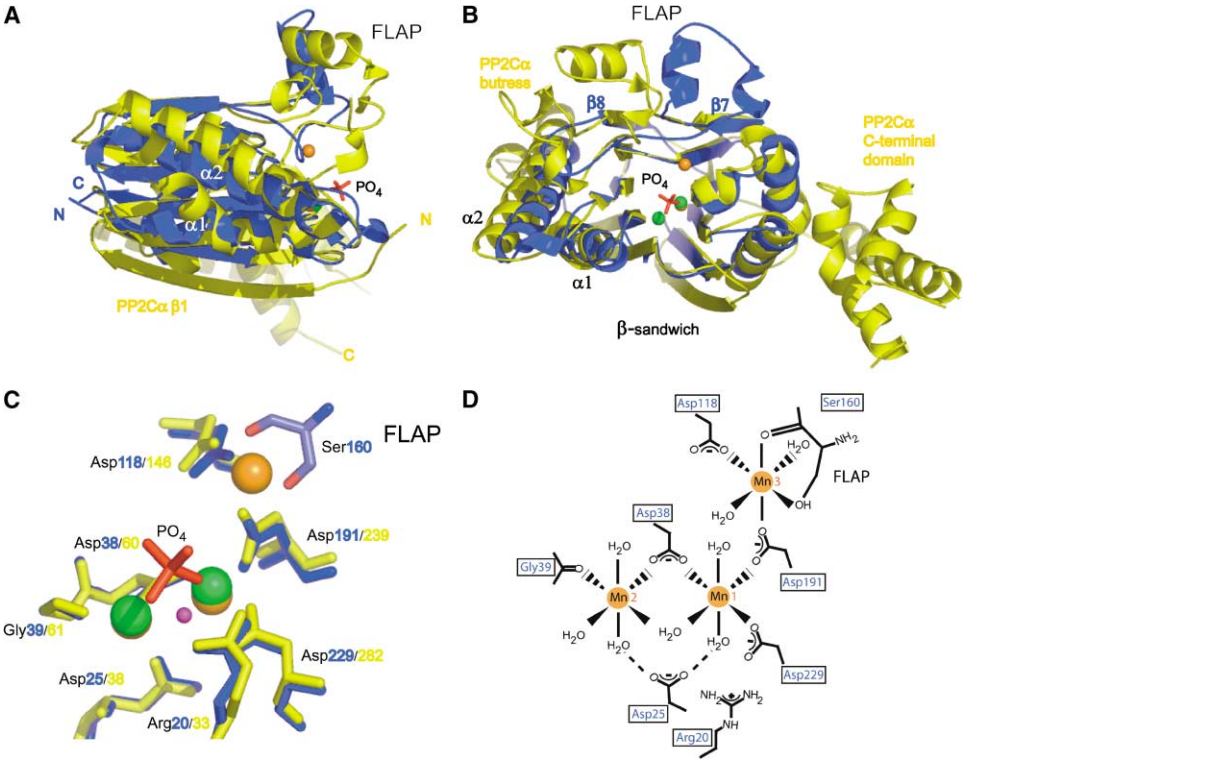

Figure 3. Conserved and Variable Features of the PP2C Phosphatases

The structures of PstP phosphatase domain (blue) and PP2Cα (yellow, 7) were superimposed using residues throughout the β sandwich core. The backbone rmsd of the common secondary structural elements excluding the flap is 2.2 Å. The product PO_4 (red stick representation) binds adjacent to the two-metal center in PP2Cα. (No phosphate was present in the PstP phosphatase-domain crystals.)

(A) Ribbon diagram shows the additional β1 strand (bottom) and C-terminal domain (back) in human PP2Cα. The N and C termini occur on opposite ends of the β sandwich in the human and *Mtb* phosphatase domains. Helix α1 (front) in the human enzyme is bent compared to helix 1 in PstP.

(B) View into the active site showing the shift in the position of the flap subdomain (top) and the position of Mn3 (orange) in PstP. Segments unique to the human enzyme include the C-terminal helical domain (right) and a loop (upper left) that buttresses the flap.

(C) Superposition of the active site residues of PstP (blue) and PP2Cα (yellow). Except for the bridging water (magenta), water molecules were omitted for clarity. The residues and side-chain positions in the two-metal centers, as well as Asp118, Asp191, and Asp195 (not shown) involved in coordinating Mn3 in PstP are strictly conserved in PP2Cα. Matching PstP Ser160 would require a conformational change in the PP2Cα flap.

(D) Schematic of the PstP active site. The invariant two-metal centers in PstP and PP2Cα show that basic features of the catalytic mechanism are conserved across the PP2C family.

The PstP sequence contains 62 additional residues (absent in this construct) linking the phosphatase domain to the predicted transmembrane helix. In contrast to the helical extension of human PP2Cα, however, this segment of PstP displays low sequence complexity in the juxtamembrane half and contains no predicted helices or recognized fold (17).

The shared secondary structural elements in the PP2C domains also show differences. For example, the first helix (PstP residues 44–62 and PP2Cα residues 65–81) is straight in the bacterial protein and bent sharply just past the middle in the human enzyme (Figure 3A). Both enzymes contain a β bulge in β strand 8, but the position of the bulge is shifted two residues along the strand in PstP. Three loops joining the secondary structural elements in the N-terminal half of the PstP sequence contain small insertions, and six PstP loops contain deletions. The bent helix 1 in the human enzyme is followed by a 13-residue loop to the next helix, while just four residues link the homologous helical hairpin in PstP.

Strikingly, a four-residue segment in the β7-β8 connector in PstP replaces a 19 residue loop in PP2Cα (Figure 3). This buttress in human PP2Cα contacts a large flap (residues 165–194) containing a helix followed by an irregular loop. Compared to the flap in the human enzyme, the PstP flap segment (residues 137–163) is two residues shorter and contains a second helix. Most notably, the flap is completely repositioned in both monomers of the PstP structure by a large hinge motion tangential to the active site (Figures 3A and 3B).

PstP Active Site

The two-metal center at the active site, including all direct ligands to the Mn^{2+} ions, is conserved in the human and bacterial PP2C phosphatases (Figure 3). The strict conservation of the nature and positioning of the residues in the dinuclear metal center supports the assignment of the bridging water molecule as the catalytic nucleophile (Das et al., 1996). This water molecule is positioned 4.1 Å from the product phosphate in the

Table 2. Steady-State Kinetic Parameters for PstP Variants at pH 7.5 and 25°C

PstP Variant	Km (Mn^{2+}), mM	Km (pNPP), mM	kcat (pNPP), min^{-1}
Wild-type	3.7 ± 0.4	1.7 ± 0.2	6.2 ± 0.2
Ser160Ala	4.8 ± 0.6	2.3 ± 0.2	6.5 ± 0.1
Asp118Asn	14.6 ± 5.4	3.2 ± 0.4	7.0 ± 0.3
Ser160Ala/Asp118Asn	12.8 ± 4.4	2.7 ± 0.6	7.4 ± 0.5

PP2Cα structure. Asp38 (like PP2Cα Asp60) provides equatorial ligands that bridge the two metals on the side opposite the bridging water. The PstP structure also shows that Asp229, like Asp282 in PP2Cα, is positioned to accept a proton from the bridging water molecule. PstP Arg20 is positioned like PP2Cα Arg33 to bind the phosphate group. Mutations of these conserved residues dramatically reduced the activity of PP2Cα (Jackson et al., 2003), consistent with their conserved structural arrangement.

PstP, however, contains no structural analog of PP2Cα His62, which has been proposed on the basis of mutagenesis, pH-rate profiles, and Brönsted analysis to act as the general acid (Jackson et al., 2003). The sequence 60-AspGlyHis-62 in PP2Cα is not found in the bacterial PP2C phosphatases, which nearly universally contain a three-residue insertion at this position. This longer sequence in PstP, 38-AspGlyMetGlyGlyHis-43, moves His43 7.2 Å away from the bridging water nucleophile compared to the position of His62 in PP2Cα. Gln, Glu, or Gly replace PstP His43 in at least four bacterial PP2C homologs, although the catalytic activities of these proteins are unknown. Thus, a general acid that is universal in the PP2C family was not identified directly by comparison of the PstP and PP2Cα structures.

In dramatic contrast to the two-metal center in PP2Cα, PstP contains a third metal ion located 5.6 and 8.3 Å from Mn1 and Mn2, respectively (Figure 3). Atomic absorption spectroscopy (data not shown) and X-ray data collected on the Mn edge (Figure 3C) indicated that all three metal ions are Mn^{2+}. Mn3 shows higher electron density and a lower B value than Mn2 in both molecules in the asymmetric unit, indicating that Mn3 is highly occupied. Mn3 binds PstP through Asp118, Ser160, Asp191, and two equatorial water molecules (Figures 3C and 3D). Asp195 forms hydrogen bonds that position the Ser160 hydroxyl group, as well as one of the water ligands. Asp118 occurs in an unusual buried turn that is conserved in human PP2Cα. Asp191 contributes an axial ligand for Mn3 and an equatorial ligand to Mn1, bridging Mn3 and the two-metal center.

Asp118 and Asp191, two of the three residues bonded to Mn3 in PstP, are strictly conserved in human PP2Cα (Figure 1) and throughout the PP2C family. In the bacterial PP2C homologs, Ser, Asn, His, or Arg commonly occur at the position of Ser160, the third Mn3 ligand in PstP. No third metal, however, was observed in the human enzyme structure. The human PP2Cα structure was determined at a pH (5.0) where the enzyme shows little activity (pKa = 7.4) (Fjeld & Denu, 1999). The difference in metal binding may be due to the difference in the location of the flap, which is positioned in PP2Cα out of reach of the third Mn site, in contact with the long β7-β8 buttressing loop that is absent from the bacterial enzyme (Figures 1 and 3B). In addition, the flap in the human enzyme adopts a distinct conformation that places Ser190, which occurs in a similar sequence element as PstP Ser160 (Figure 1), in a different local structural position. Thus, a tertiary conformational change in the flap, as well as a large hinge motion, would be needed to provide a Mn3 ligand in human PP2Cα analogous to PstP Ser160. These results suggest that the flap may be a versatile structural element that occupies distinct positions in different PP2C phosphatases. Alternatively, the flap may constitute a mobile segment coupled conformationally to the binding of Mn3.

To explore the roles of the third Mn^{2+} in PstP, we characterized the effects of mutations of the Mn3 ligands Ser160 and Asp118 (Table 2). Consistent with previous measurements on the wild-type enzyme (Chopra et al., 2003) and PP2Cα (Fjeld and Denu, 1999), the PstP phosphatase domain showed a Km for Mn^{2+} in the mM range in the reaction of the classic, noncognate substrate, pNPP. The Ser160Ala mutation in the flap had little effect on pNPP kinetics. In contrast, the Asp118Asn and Asp118Asn/Ser160Ala mutants showed higher Michaelis constants for Mn^{2+}, but the mutations had little effect on kcat for pNPP (Table 2).

Functional Implications

The structure of PstP reveals a conserved fold and a structurally invariant dinuclear Mn^{2+} center that forms the core of the PP2C enzymes. At the same time, the third Mn^{2+} observed in PstP and the large difference in the position of the flap compared to human PP2Cα identify distinctive elements that expand the framework for understanding the mechanisms of PP2C phosphatases. Sequence conservation among bacterial PP2Cs is localized to a large "hemisphere" surrounding the active site and the flap (Figure 4). The flap creates deep grooves that converge on the metal center (Figure 4). The position of the metal center at the confluence of these surface channels suggests that they may function as binding sites for substrate phosphopeptides. The PstP structure suggests that further work on PP2C-family enzymes is needed to explore the generality of the Mn3 site and to determine whether the flap is a static or mobile element.

From a structural perspective, Mn3 is coupled to Mn1 through the shared Asp191 and to the flap through Ser160 (Figures 3C and 3D). Consistent with a role in tuning metal affinity, the Asp118Asn mutation in the Mn3 binding site increased the Mn^{2+} concentration required for pNPP turnover (Table 2). Although this effect was modest, the reaction of wild-type PstP required high (mM) concentrations of Mn^{2+} (Table 2), suggesting that metal binding could play a regulatory role. Availability of Mn^{2+} has been proposed to raise free iron levels and

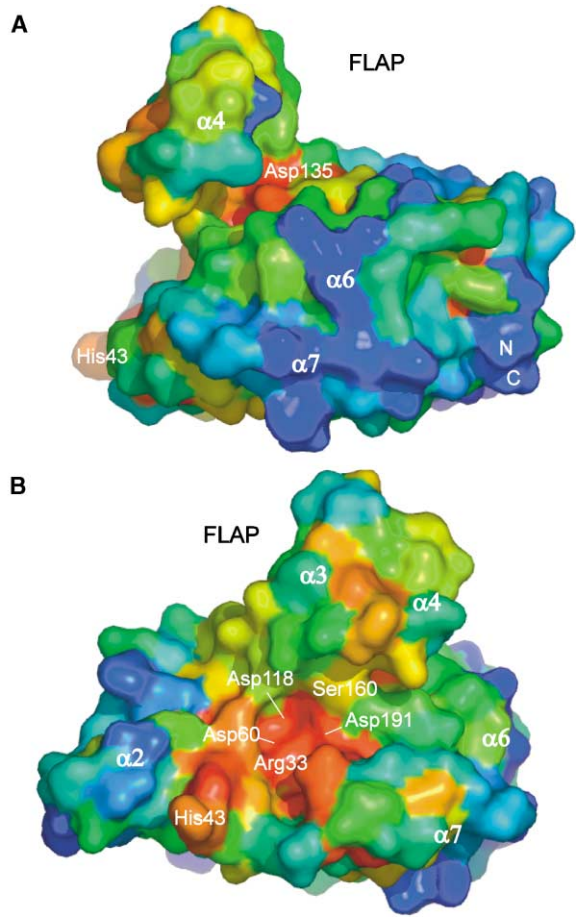

Figure 4. Surface Sequence Conservation in Bacterial PP2C Phosphatases Clusters around the Active Site and Flap Regions of PstP

The PstP surface was colored from red (high) to blue (low) corresponding to the level of sequence homology among 64 predicted bacterial PP2C phosphatases. Representative sequences were selected from 167 homologs (E value < 0.001) identified using a BLAST search of 240 microbial genomes. The levels of sequence identity with the *Mtb* PstP catalytic domain ranged from 99% and 95%, respectively, for the *M. bovis* and *M. leprae* PstPs to 26% (E value $= 6 \times 10^{-5}$) for a predicted phosphatase from *Pseudomonas fluorescens*. PstP residues are indicated in the one-letter code.

(A) View corresponding to Figure 2B showing high variability (right) in much of the surface of the β sandwich distal to the active site. A deep groove separates the β sandwich and the flap (top).

(B) View into the active site (corresponding to Figure 2C) shows extensive conservation of the active site, the flap, and the grooves emanating from the metal centers. This conservation pattern suggests that this surface of the PstP phosphatase domain plays important roles in substrate recognition, catalysis, and regulation.

to directly activate the *B. subtilis* PP2C protein phosphatase, RsbU, which in turn activates sigmaB, a mediator of the stress response (Guedon et al., 2003). *Mtb* grows in vivo within macrophage phagosomes, which are thought to contain limiting concentrations of certain divalent cations, including Fe^{2+} (Bellamy, 2003; Schnappinger et al., 2003). In this context, it is striking that the catalytic domains of PstP and several of the STPKs display a requirement for Mn^{2+} (Boitel et al., 2003; Chopra et al., 2003; Peirs et al., 1997; Av-Gay et al., 1999; Koul et al., 2001; Chaba et al., 2002). In principle, this Mn^{2+} dependence may globally couple the signaling activities of the *Mtb* STPK systems to the growth environment.

Alternatively, by influencing the position of the flap or by providing an extended binding site for diphosphorylated peptides, Mn3 may help mediate recognition of diverse, cognate phosphoprotein substrates. PstP efficiently dephosphorylates a variety of singly and multiply phosphorylated proteins, including PknA, PknB (Boitel et al., 2003, Chopra et al., 2003), and other *Mtb* STPK domains (data not shown). STPK dephosphorylation simultaneously abolishes binding sites for substrates containing FHA domains (Molle et al., 2003) and substantially reduces protein kinase activity (Boitel et al., 2003). Thus, Mn3 and the flap may enable PstP to modulate different signaling pathways.

Experimental Procedures

Amplification and Cloning

Using sticky-end PCR (Pham et al., 1998) to amplify genomic DNA of *M. tuberculosis* HRv37, an expression vector for PstP residues 1–237 followed by a C-terminal His tag, LEHHHHHH, was made in pET24b (Novagen). Mutagenesis was carried out using the QuikChange method (Stratagene). Constructs and mutants were confirmed by DNA sequencing.

Expression and Purification of PstP

PstP variants and selenomethionine (SeMet)-labeled PstP were expressed as described (Young et al., 2003; van Duyne et al., 1993) in BL21-CodonPlus (DE3) cells (Stratagene) containing the expression plasmid. Log-phase cells were induced with 250 μM IPTG for 24 hr at 18°C. The cells were harvested by centrifugation and lysed using sonication on ice in 300 mM NaCl, 20 mM Tris (pH 7.5), 0.5 mM tris(2-carboxyethyl)phosphine hydrochloride (TCEP), and 5 mM L-Met. The lysate was clarified by centrifugation and loaded on a 5 ml immobilized metal affinity chromatography column (Amersham-Pharmacia) equilibrated with 50 mM Ni_2SO_4. The protein was eluted using a 0–300 mM imidazole gradient in 110 ml. The protein fractions were concentrated and separated on a HiLoad 26/60 Superdex 75 (Amersham-Pharmacia) gel exclusion column equilibrated with 50 mM NaCl, 20 mM Tris (pH 7.5), and 0.5 mM TCEP. The PstP peak was loaded onto a 5 ml HiTrap Q Sepharose ion-exchange (Amersham-Pharmacia) column and eluted with a 0.05–1 M NaCl gradient in 100 ml. The purified protein was dialyzed into buffer containing 50 mM NaCl, 20 mM Tris (pH 7.5), 0.5 mM TCEP, and 1 mM $MnCl_2$.

Crystallization

PstP (10 mg ml^{-1}) was crystallized at 18°C by vapor diffusion using hanging drops containing a 1:1 mixture of protein and reservoir solution of 8% PEG-10,000, 0.1 M sodium cacodylate (pH 6.0). Prior to X-ray data collection, the crystals were soaked in a solution containing 8% PEG-10,000, 0.1 M sodium cacodylate, 0.5 mM TCEP, and 25% ethylene glycol for 1 min, mounted on a loop, and frozen in liquid N_2. To test catalytic competence, SeMet PstP crystals were transferred to a solution containing 10% PEG-10,000, 0.1 M HEPES (pH 7.5), and 25 mM pNPP at 25°C and incubated for 1 hr. The production of bright yellow p-nitrophenol was visualized by eye.

Structure Determination

Using beamline 8.3.1 at the Lawrence Berkeley National Laboratory Advanced Light Source, X-ray data were collected from a single crystal of SeMet-labeled PstP at 100 K at the Se peak, low-remote, and high-remote energies. To identify the bound metal ions, data also were collected at the Mn^{2+} absorbtion peak at 8926 eV. The crystals had the symmetry of space group $P2_1$ with two PstP monomers in the asymmetric unit. Data were processed to 1.95 Å resolution using HKL2000 (Otwinowkski and Minor, 1997). The Elves automation program (Holton and Alber, 2004) found 10 of the 12 Se sites

and calculated electron density maps. The initial model was built using ARP/wARP (Morris et al., 2002).

The structure was refined at 1.95 Å resolution using REFMAC (Murshudov et al., 1997). The R_{free} was calculated using a random 5% of the data. The model was completed with cycles of rebuilding using O (Jones et al., 1991) and refinement using REFMAC. The final model contains two monomers of PstP (residues 6–237 and 5–237), the first three residues of each His tag, six Mn^{2+} ions, and 241 water molecules per asymmetric unit. The stereochemistry of the model was monitored using PROCHECK (Laskowski et al., 1993). No residues had disallowed main chain dihedral angles, and the G factor of the model (G = 0.2) was better than most structures refined at this resolution.

Atomic Absorption Spectroscopy

Native protein equilibrated with 1 mM $MnCl_2$ was analyzed by inductively coupled plasma-atomic emission spectroscopy (ICP-AES) using a Perkin Elmer Optima 3000DV spectrophotometer. Samples were analyzed for ppm and ppb quantities of V, Cr, Mn, Fe, Co, Ni, Cu, and Zn. Only Mn was detected in significant quantities.

Enzyme Kinetics

The purified wild-type or mutant proteins were exchanged into reaction buffer containing 50 mM NaCl, 20 mM Tris, pH 7.5, and 0.5 mM TCEP. The enzymes were incubated with various amounts of pNPP, and reaction progress data were collected at 405 nM and 25°C using a SPECTRAmax 190 spectrophotometer (Molecular Devices). Kinetic constants were calculated using SigmaPlot (Systat Software Inc.).

In order to determine the effect of metal concentration on enzyme activity, various amounts of $MnCl_2$ were mixed with 50 mM pNPP. The reaction was initiated by adding enzyme at a final concentration of 1 μM, and the assay was monitored continuously for several minutes. To determine the k_{cat} and K_m values for pNPP, eight substrate dilutions were made. Reactions contained 100 mM $MnCl_2$ and a final enzyme concentration of 1 μM.

Acknowledgments

We thank J. Holton for help with X-ray data collection and S. Mills for help with atomic absorbtion measurements. We benefited from thoughtful discussions with E. Skordalakes, J. Mougous, Y. Feng, and M. Marletta. We are indebted to T. Terwilliger and the TB Structural Genomics Consortium for support. We gratefully acknowledge a Ford Foundation Pre-doctoral Fellowship to K.E.P. This work was supported by a grant from the NIH. The Advanced Light Source Beamline 8.3.1 was funded by the NSF, the University of California, and Henry Wheeler.

Received: August 2, 2004
Revised: September 3, 2004
Accepted: September 3, 2004
Published: November 9, 2004

References

Av-Gay, Y., and Everett, M. (2000). The eukaryotic-like Ser/Thr protein kinases of *Mycobacterium tuberculosis*. Trends Microbiol. *8*, 238–244.

Av-Gay, Y., Jamil, S., and Drews, S.J. (1999). Expression and characterization of the Mycobacterium tuberculosis serine/threonine protein kinase PknB. Infect. Immun. *67*, 5676–5682.

Barford, D., Das, A.K., and Egloff, M.P. (1998). The structure and mechanism of protein phosphatases: insights into catalysis and regulation. Annu. Rev. Biophys. Biomol. Struct. *27*, 133–164.

Bellamy, R. (2003). Susceptibility to mycobacterial infections: the importance of host genetics. Genes Immun. *4*, 4–11.

Boitel, B., Ortiz-Lombardia, M., Duran, R., Pompeo, F., Cole, S.T., Cervenansky, C., and Alzari, P.M. (2003). PknB kinase activity is regulated by phosphorylation in two Thr residues and dephosphorylation by PstP, the cognate phospho-Ser/Thr phosphatase, in *Mycobacterium tuberculosis*. Mol. Microbiol. *49*, 1493–1508.

Bhaduri, A., and Sowdhamini, R. (2003). A genome-wide survey of human tyrosine phosphatases. Protein Eng. *16*, 881–888.

Chaba, R., Raje, M., and Chakraborti, P.K. (2002). Evidence that a eukaryotic-type serine/threonine protein kinase from Mycobacterium tuberculosis regulates morphological changes associated with cell division. Eur. J. Biochem. *269*, 1078–1085.

Chopra, P., Singh, B., Singh, R., Vohra, R., Koul, A., Meena, L.S., Koduri, H., Ghildiyal, M., Deol, P., Das, T.K., et al. (2003). Phosphoprotein phosphatase of *Mycobacterium tuberculosis* dephosphorylates serine-threonine kinases PknA and PknB. Biochem. Biophys. Res. Commun. *311*, 112–120.

Cole, S.T., Brosch, R., Parkhill, J., Garnier, T., Churcher, C., Harris, D., Gordon, S.V., Eiglmeier, K., Gas, S., Barry, C.E., III, et al. (2000). Deciphering the biology of *Mycobacterium tuberculosis* from the complete genome sequence. Nature *393*, 537–544.

Das, A.K., Helps, N.R., Cohen, P.T., and Barford, D. (1996). Crystal structure of the protein serine/threonine phosphatase 2C at 2.0 A resolution. EMBO J. *15*, 6798–6809.

Fjeld, C.C., and Denu, J.M. (1999). Kinetic analysis of human serine/threonine protein phosphatase 2Cα. J. Biol. Chem. *274*, 20336–20343.

Guedon, E., Moore, C.M., Que, Q., Wang, T., Ye, R.W., and Helmann, J.D. (2003). The global transcriptional response of *Bacillus subtilis* to manganese involves the MntR, Fur, TnrA and sigmaB regulons. Mol. Microbiol. *49*, 1477–1491.

Holton, J.M., and Alber, T. (2004). Automated protein crystal structure determination using Elves. Proc. Natl. Acad. Sci. USA *101*, 1537–1542.

Jackson, M.D., and Denu, J.M. (2001). Molecular reactions of protein phosphatases–insights from structure and chemistry. Chem. Rev. *10*, 2313–2340.

Jackson, M.D., Fjeld, C.C., and Denu, J.M. (2003). Probing the function of conserved residues in the serine/threonine phosphatase PP2Cα. Biochemistry *42*, 8513–8521.

Jones, T.A., Zou, J.Y., Cowan, S.W., and Kjeldgaard, M. (1991). Improved methods for building protein models in electron density maps and the location of errors in these models. Acta Crystallogr. *A47*, 110–119.

Kelley, L.A., MacCallum, R.M., and Sternberg, M.J. (2000). Enhanced genome annotation using structural profiles in the program 3D-PSSM. J. Mol. Biol. *299*, 499–520.

Kennelly, P.J. (2002). Protein kinases and protein phosphatases in prokaryotes: a genomic perspective. FEMS Microbiol. Lett. *206*, 1–8.

Kerk, D., Bulgrien, J., Smith, D.W., Barsam, B., Veretnik, S., and Gribskov, M. (2002). The complement of protein phosphatase catalytic subunits encoded in the genome of *Arabidopsis*. Plant Physiol. *129*, 908–925.

Koul, A., Choidas, A, Tyagi, A.K., Drlica, K., Singh, Y., and Ullrich, A. (2001). Serine/threonine protein kinases PknF and PknG of Mycobacterium tuberculosis: characterization and localization. Microbiology *147*, 2307–2314.

Laskowski, R.A., MacArthur, M.W., Moss, D.S., and Thornton, J.M. (1993). PROCHECK: a program to check the stereochemical quality of protein structure. J. Appl. Crystallogr. *26*, 283–291.

McCarty, D.R., and Chory, J. (2000). Conservation and innovation in plant signaling pathways. Cell *103*, 201–209.

Molle, V., Kremer, L., Girard-Blanc, C., Besra, G.S., Cozzone, A.J., and Prost, J.F. (2003). An FHA phosphoprotein recognition domain mediates protein EmbR phosphorylation by PknH, a Ser/Thr protein kinase from *Mycobacterium tuberculosis*. Biochemistry *42*, 15300–15309.

Morris, R.J., Perrakis, A., and Lamzin, V.S. (2002). ARP/wARP's model-building algorithms. I. The main chain. Acta Crystallogr. *D58*, 968–975.

Murshudov, G.N., Vagin, A.A., and Dodson, E.J. (1997). Refinement of macromolecular structures by the maximum-likelihood method. Acta Crystallogr. *D53*, 240–255.

Otwinowski, Z., and Minor, W. (1997). Processing of x-ray diffraction

data collected in oscillation mode. In Methods in Enzymology, Volume 276, C.W. Carter, Jr. and R. Sweet, eds. (New York: Academic Press), pp. 307–326.

Peirs, P., De Wit, L., Braibant, M., Huygen, K., and Content, J. (1997). A serine/threonine protein kinase from Mycobacterium tuberculosis. Eur. J. Biochem. *244*, 604–612.

Pham, K., LaForge, K.S., and Kreek, M.J. (1998). Sticky-end PCR: new method for subcloning. Biotechniques *25*, 206–208.

Russell, D.G. (2001). *Mycobacterium tuberculosis*: here today, and here tomorrow. Nat. Rev. Mol. Cell Biol. *2*, 569–577.

Schnappinger, D., Ehrt, S., Voskuil, M.I., Liu, Y., Mangan, J.A., Monahan, I.M., Dolganov, G., Efron, B., Butcher, P.D., Nathan, C., and Schoolnik, G.K. (2003). Transcriptional adaptation of *Mycobacterium tuberculosis* within macrophages: insights into the phagosomal environment. J. Exp. Med. *198*, 693–704.

van Duyne, G.D., Standaert, R.F., Karplus, P.A., Schreiber, S.L., and Clardy, J. (1993). Atomic structures of the human immunophilin FKBP-12 complexes with FK506 and rapamycin. J. Mol. Biol. *229*, 105–124.

Walburger, A., Koul, A., Ferrari, G., Nguyen, L., Prescianotto-Baschong, C., Huygen, K., Klebl, B., Thompson, C., Bacher, G., and Pieters, J. (2004). Protein kinase G from pathogenic mycobacteria promotes survival within macrophages. Science *304*, 1800–1804.

Wang, W.Q., Sun, J.P., and Zhang, Z.Y. (2003). An overview of the protein tyrosine phosphatase superfamily. Curr. Top. Med. Chem. *3*, 739–748.

Young, T.A., Delagoutte, B., Endrizzi, J.A., Falick, A.M., and Alber, T. (2003). Structure of Mycobacterium tuberculosis PknB supports a universal activation mechanism for Ser/Thr protein kinases. Nat. Struct. Biol. *10*, 168–174.

Accession Numbers

The coordinates and structure factors were deposited in the Protein Data Bank with accession number 1TX0.